Dynamics of linear ITG modes in the presence of ExB flow shear

V.I. Dagnelie[1,2], J. Citrin[1], F. Jenko[3], M.J. Pueschel[4,5], T. Görler[3], D. Told[3] and H. Doerk[3]

[1]DIFFER - Dutch Institute for Fundamental Energy Research, De Zaale 20, 5612AJ Eindhoven, The Netherlands
[2]Institute for Theoretical Physics, Utrecht University, Princetonplein 5, 3584CC Utrecht, The Netherlands
[3]Max Planck Institute for Plasma Physics, Boltzmannstr. 2, 85748 Garching, Germany
[4]Department of Physics, University of Wisconsin-Madison, Madison, Wisconsin 53706, USA
[5]Institute for Fusion Studies, University of Texas at Austin, 1 University Station, C1500, Austin, Texas

Abstract

Inside a toroidal nuclear fusion reactor, unstable plasma modes driven by a radial ion temperature gradient (ITG) can be stabilized by rotational flow shear. In this study, these rotational modes are solved from the linear gyrokinetic equations and scrutinized in ballooning space. The effect of flow shear is immediately apparent in ballooning space, as is the difference in stabilization between kinetic and adiabatic electron calculations at low magnetic shear $\hat{s}$ (mode quench occurs at much lower flow shear in the adiabatic case). Modes consistently equilibrate to some shape in ballooning space, even when they exhibit Floquet fluctuations in time. To gain physical insight into the mechanics of flow-shear stabilization and Floquet fluctuations, a toy model is created. The full rotational ITG solution is decomposed into shearless modes and flow-shear modifications. The model reproduces mode structures in ballooning space, Floquet fluctuations and the stabilizing impact of flow shear.

1 Introduction

Turbulent transport is the primary mechanism which limits plasma core confinement in tokamaks [1]. Among the main instability branches which drive the turbulence are ion-temperature-gradient (ITG) modes [2, 3]. These linear modes are characterized by a critical threshold in ion temperature gradient. At higher amplitudes the modes nonlinearly couple and eventually saturate in a quasi-stationary state. However, in the transport driving spatial scales, the linear characteristics of these modes are still evident in the nonlinear state, e.g. see [4, 5] and references therein. Thus, correct evaluation of linear mode characteristics is experimentally relevant and vital for the validity of quasilinear transport models.

Confinement improvement through turbulent transport reduction would allow smaller fusion reactors to be built for the same output fusion power. One method to mitigate or weaken the impact of ITG modes is through plasma rotation flow shear. This has been widely studied experimentally, analytically, and computationally [6, 7, 8, 9, 10, 11, 12].

In this work we investigate unstable linear ITG modes in ballooning space [13, 14], through local (flux-tube) gyrokinetic simulations with GENE [15]. The implementation of perpendicular flow shear in GENE is through time dependent shifts in radial wavenumber [16]. We focus on how this provides the stabilising effect of flow shear, reproduces Flo-

quet fluctuations in the ITG growth rates, and a strikingly different stabilisation at low magnetic shear ($\hat{s}$) when either kinetic or adiabatic electrons are applied. Finally, we attempt to capture these effects in a toy model, aiming towards implementation within reduced quasilinear transport models.

In section 2 we describe the necessary background formalism and in section 3 a novel growth rate calculation method is oulined. In section 4 the results of simulations of this study are shown. In section 5 the toy model is presented.

2 Background Theory

We describe a circular tokamak with coordinates x (radial), y (binormal), z (parallel). In this work, we use the linearized gyrokinetic framework [19] to find eigenmode solutions Φ. The electrostatic potential φ associated with the ITG instability has a distinctive spatial structure, which is continuously deformed in the presence of flow shear. Using the ballooning transformation, one may write

$$\Phi(k_x,\theta_b) = \sum_{m=-\infty}^{\infty} \int \mathrm{d}x \int \mathrm{d}y \int \mathrm{d}z \;\; \varphi(x,y,z) \; e^{i\left[m(\theta_b - z) - k_x x + C_y k_y (y - q(x)\theta_0)\right]}. \quad (1)$$

Here θ_0 is the ballooning angle of a mode Φ, the ballooning coordinate $\theta_b \in (-\infty, \infty)$ spans ballooning space, q is the safety factor, $C_y = \epsilon_t/q$ is a geometric constant (with $\epsilon_t = r/R$ the inverse aspect ratio at the radial location r of the chosen flux tube, with R the tokamak's major axis), and the sum is over all integers m. The ballooning angle and wavenumbers k are related by $k_x = -k_y \hat{s} \theta_0$, where the magnetic shear $\hat{s} = (r/q)\partial q/\partial r$. The parallel boundary condition in these coordinates states that each value of k_x can be written as $k_x = k_x' + 2\pi\hat{s}k_y$ [20]. Finally, in Gene, rotational flow shear (defined as $\gamma_E = (x/q)\partial v_{\mathrm{tor}}/\partial x$ with v_{tor} the toroidal plasma velocity) is implemented by shifting the k_x grid in time: $k_x = C_y k_y \gamma_E t/q$. By these relations, when $\hat{s} \neq 0$ and $\gamma_E \neq 0$, the quantities t, k_x and θ_0 can be translated into each other when considering a mode Φ. Because of the finite number of radial modes simulated in a numerical system, the k_x shifts are discrete, even though t is a continuous variable.

From the perturbed particle distribution function $f_{1,i}$ of species i, the perturbed plasma density is obtained by $n_{1,i} = \int \mathrm{d}^3 v f_{1,i}$. The growth rate γ in a time interval Δt is then defined by $\frac{n_{1,i}(t+\Delta t)}{n_{1,i}(t)} = e^{\gamma \Delta t}$, where the k_y dependency was omitted and an average is taken over k_x values. As such, a mode's growth rate can be obtained from Gene simulations at each time step. A mode Φ is considered unstable if its growth rate $\gamma > 0$. Without flow shear, growth rates converge after some time. With flow shear, under certain circumstances, so-called Floquet fluctuations occur: the growth rate fluctuates periodically in time around some average.

3 Growth rates: τ_{AC} method

It is often observed in the literature that linear growth rates in the presence of flow shear are calculated from an average of the fluctuating Floquet mode (we call this the γ_{avg} method). However, the timescale of this averaging is much greater than the non-linear decorrelation time, which raises doubts whether this averaging leads to a physically relevant quantity. In this work, we therefore use the τ_{AC} method, similar to that proposed in [21, 22]. This approach assumes that the relevant timescale for growth rate calculations is the non-linear decorrelation time. Next, it is assumed that this timescale at a given spatial scale is given by $1/\gamma_k$, where γ_k is the growth rate of the most unstable mode at the respective spatial scale. As such, the time scale indeed corresponds to the growth time needed to enter a nonlinear regime. It was shown that this assumption is works well at low values of k_y such as used in this work [23]. The proposed method is to iteratively calculate the growth rate using an adaptive time window until the width of the time window converges to the inverse growth rate calculated. This is illustrated in Fig. 1, where a mode amplitude timetrace is shown for a Cyclone Base Case (CBC) linear simulation with kinetic electrons, $\gamma_E = 0.3$, and $k_y = 0.3$. CBC parameters are circular geometry,

$\hat{s}/q = 0.8/1.4$, $\epsilon_t = 0.18$, $R/L_n = 2.2$, $R/L_T = 6.75$, (where L_n and L_T are the length scales corresponding to the plasma density and temperature gradients, respectively). An automated routine is written in which a time window scans over the amplitude timetrace. At each point in the scan growth rates are defined as $\gamma_k(t_1, \Delta t) = \ln\left[n(t_1 + \Delta t)/n(t_1)\right]/\Delta t$, in which t_1 is the starting point of the time window, Δt is the time window width, and n is the plasma density (other fields and moments can be chosen here; all converge to the same growth rate). For a given Δt, the averaged growth rate $\gamma_k(\Delta t)$ is then defined as an average over the $\gamma_k(t_1, \Delta t)$ peaks in the t_1 scan over the timetrace, which smooths out any variations in the peaks which may arise due to the discrete k_x shifts present in the implementation of the flow shear in GENE [16].

The assumption that the physical growth rate value is weighted towards the peak growth rates over a Floquet cycle is not fully justified in this work, but it is based on the following intuition: the injected energy into the system from the original instability is with θ_0, due to the typical maximum growth rate at $k_x = 0$ of these modes. If the short nonlinear decorrelation time (itself assumed to be $1/\gamma_k$) is then short enough for a mode not to traverse a full Floquet cycle, then it is logical that the effective growth rate is still weighted towards the $k_x = 0$ values.

The final γ_k is then obtained by iterating this procedure and adapting Δt, until convergence is achieved when $|1 - \gamma_k \Delta t| < \delta$. The convergence criterion has been chosen as $\delta = 0.02$ for this work. The time window displayed in Fig. 1(a) (bounded by the red lines) is at a position corresponding to the first $\gamma_k(t_1, \Delta t)$ peak in the t_1 scan for the converged Δt for this particular case.

Growth rate calculations using the τ_{AC} method are displayed in Fig. 2 at $R/L_{T\mathrm{i}} = 8.75$ and for both adiabatic and kinetic electrons. In the kinetic electron case, $R/L_{T\mathrm{e}} = 4$, such that we avoid a sub-dominant electron mode which masks the ITG quenching at high γ_E. For both adiabatic and kinetic electrons, the fundamental quench behavior is very similar, with the quench occurring at $\gamma_E \approx 2\gamma_0$, where γ_0 is the static growth rate. However, for low γ_E the initial sharp drop in growth rate previously seen is now not

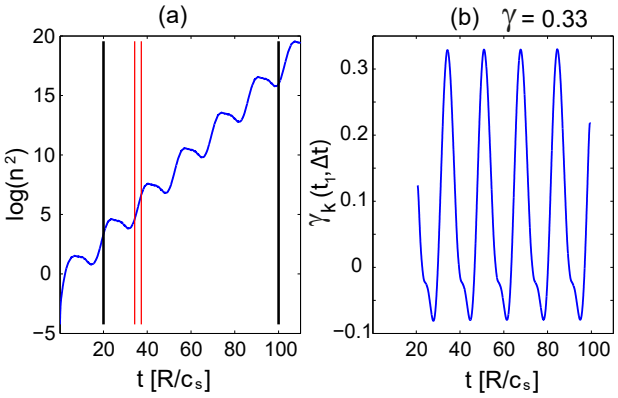

Fig. 1: **(a)** Mode amplitude timetrace, with growth rates analyzed between the black lines and the calculated converged time window width $\Delta t = 1/\gamma_k$ between red lines.
(b) Corresponding local growth rates $\gamma_k(t1, \Delta t)$. The resulting final growth rate is the peak average $\gamma = 0.33$.

so apparent, and much smoother profiles result. At higher γ_E, the growth rates are sufficiently low that the time window in the τ_{AC} method averages over a number of cycles, and is effectively equivalent to a long time-scale averaging (γ_{avg}) method.

The τ_{AC} method can be applied for calculating effective growth rates in the presence of flow shear, of the form $\gamma_{\mathrm{eff}} = \gamma - \alpha\gamma_E$, e.g. as in [17]. Multiple linear gyrokinetic runs with the τ_{AC} method can be applied to calculate the parameter dependencies of the α factor in setting γ_{eff}, potentially leading to a simple but accurate method for setting the flow-shear impact in quasilinear transport models. This will be explored in future work.

For quenched modes ($\gamma_{\mathrm{avg}} < 0$), there are often no clear converged or periodic growth rates, so that the τ_{AC} method cannot be used. An approximate average growth rate is then obtained by using the γ_{avg} method.

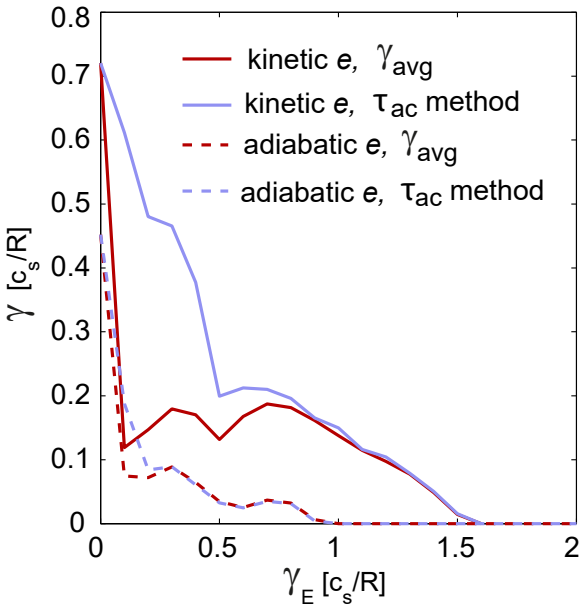

Fig. 2: Comparison of growth rates with the γ_{avg} and the τ_{AC} method with $R/L_{T\mathrm{e}} = 4$ for kinetic electrons, $R/L_{T\mathrm{e}} = 8.75$ for adiabatic electrons and $R/L_{T\mathrm{i}} = 8.75$ for both cases.

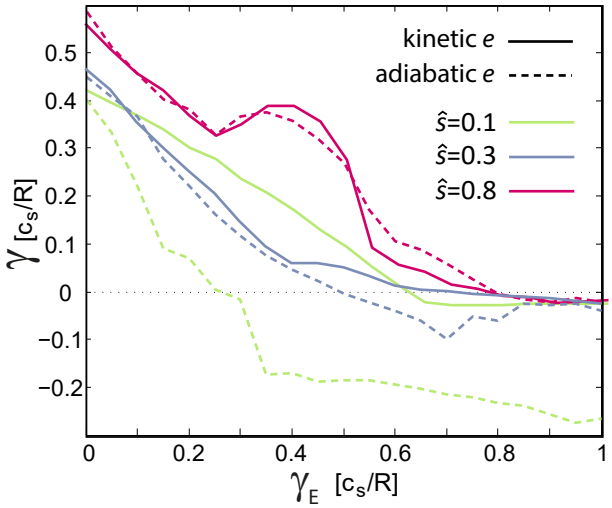

Fig. 3: Growth rates of ITG modes at various values of $\hat{s}$, for kinetic electrons (solid) with $R/L_{T\mathrm{i}} = 6.75$ and adiabatic electrons (dashed) with $R/L_{T\mathrm{i}} = 10$.

4 Simulations

Simulations are always carried out at Cyclone Base Case (CBC) parameters with modified temperature gradients. Typical grid sizes are 90 for k_x, 24 for z, 32 for $v_\parallel$ and 8 for μ. Typically, $\Delta k_x \approx 0.1$. This small k_x step size is necessary in the presence of flow shear, to make the jumps in the k_x grid small enough. Certainly, Δk_x must be smaller than the distance between modes that are coupled by the parallel boundary condition. Convergence is checked by decreasing grid sizes until growth rates start to change significantly, and then simulating well above these thresholds.

Shown in Fig. 3 is the averaged growth rate of linear ITG modes vs. flow shear, at several values of magnetic shear $\hat{s}$. This is done using either kinetic electrons with $R/L_{T_\mathrm{i}} = 6.75$ or adiabatic electrons with $R/L_{T_\mathrm{i}} = 10$, where the temperature gradient is chosen differently to match rotationless growth rates. At high $\hat{s} = 0.8$ the reduction of unstable growth rates is similar between the two cases, but at low $\hat{s} = 0.1$ the ITG modes are quenched at much lower flow shear when adiabatic electrons are used. This may impact previous research done under these circumstances (low $\hat{s}$, adiabatic electrons) [18, 12]. To investigate the origin of this difference, we visualize ITG modes at both high and low magnetic shear.

In Fig. 4, we show ITG modes in ballooning space for several values of flow shear. An unexpected feature of these visualizations is that modes equilibrate to some shape in ballooning space; they do not shift around but merely grow and/or shrink maintaining practically the same shape, even when large Floquet fluctuating are present. This is shown in Fig. 6. Shapes are seen to jump in time by the discrete nature of the GENE flow shear implementation, but this effect is not physical; the jumps decrease when smaller k_x step sizes are chosen.

When $\hat{s} = 0.8$ (Fig. 4(a)), structures are sharply peaked around $\theta_b = 0$. Growth rates are gradually reduced as flow shear increases. There is little difference between kinetic and adiabatic electron simu-

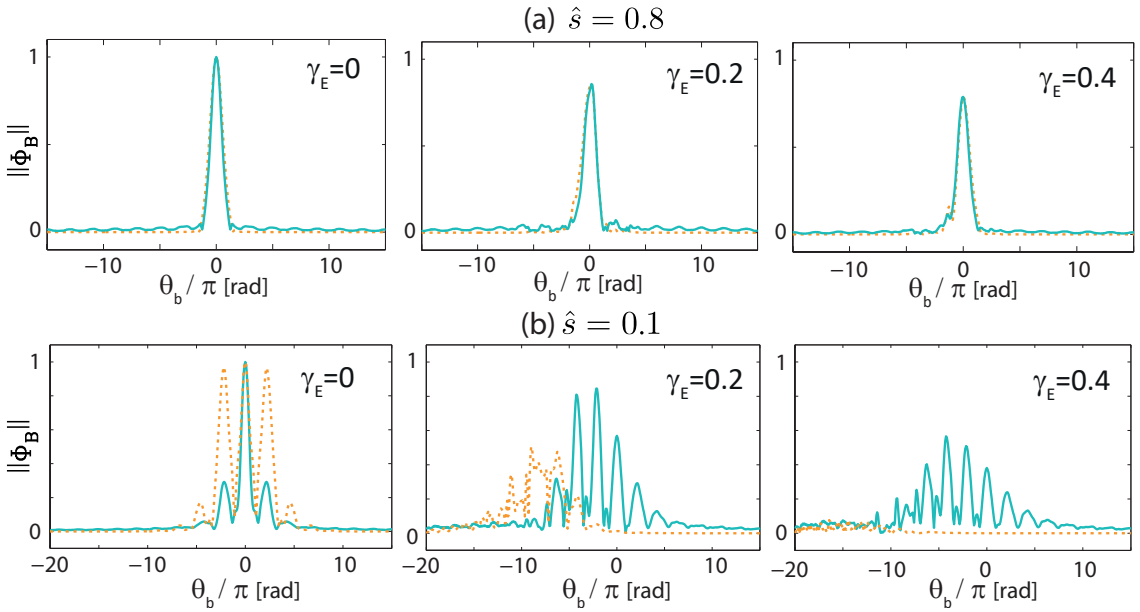

Fig. 4: Impact of flow shear on ITG modes in ballooning space, for **(a)** $\hat{s} = 0.8$ and **b** $\hat{s} = 0.1$. Solid lines correspond to kinetic electrons and dashed lines to adiabatic electrons.

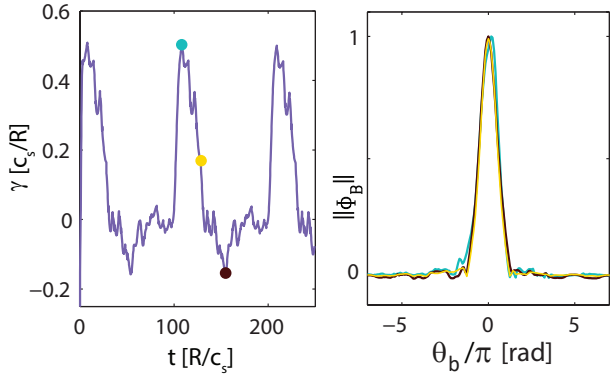

Fig. 6: Floquet modes in ITG growth with $\gamma_E = 0.1$ (left), and normalized mode structures in ballooning space at several times (right). The mode structures are measured at the times of the colored dots in the left pane, indicating the preservation of their shape.

lations, except that at large θ_b, adiabatic modes $|\Phi|$ drop to values several orders of magnitude smaller values than kinetic modes. This slight difference is consistently observed throughout all simulations in this work. At $\hat{s} = 0.1$ (Fig. 4(b)), structures are more spread out over ballooning space, since, with our definitions, at low $\hat{s}$ the same coverage in k_x space (compared to high $\hat{s}$) corresponds to a larger range in ballooning space. As flow shear is increased, the distribution widens further and shifts towards negative ballooning space (by continuous shifting of the k_x grid), without being quenched as in the high $\hat{s}$ case. Also, in the shift we observe a clear difference between kinetic and adiabatic electron simulations: adiabatic modes experience a shift to negative ballooning space by flow shear much quicker than kinetic modes. At these higher ballooning coordinates (thus higher radial wavenumbers) the modes are consequently quenched more, in line with the findings of Fig. 3.

As outlined before, ITG modes $|\Phi|$ are continuously shifted over the k_x grid (thus also through ballooning space) by flow shear. Alternatively, we can take

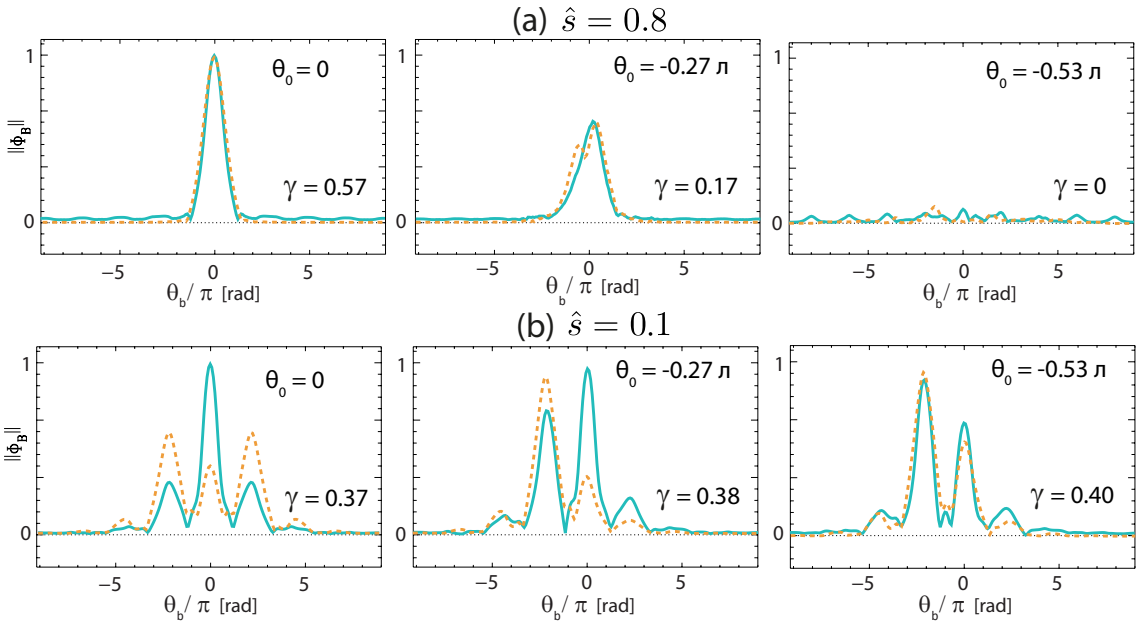

Fig. 5: Impact of shifted ballooning angle on rotationless ITG modes ϕ_n, for **(a)** $\hat{s} = 0.8$ and **b** $\hat{s} = 0.1$. Solid lines correspond to kinetic electrons and dashed lines to adiabatic electrons.

a mode without flow shear and let it evolve at a fixed shifted k_x grid (=shifted ballooning angle). Such modes we call ϕ_n, where n denotes the mode's ballooning angle, defined via $\theta_0 = -\pi n/8$. In Fig. 5 we simulate modes ϕ_n for $n \in [0, 8]$, such that we cover ballooning angles $\theta_0 \in [-\pi, 0]$. By parallel symmetry these are equal to the mirror images of the modes with $\theta_0 \in [0, \pi]$. In Fig. 5(a) these modes are shown for $\hat{s} = 0.8$. Structures are again sharply peaked around $\theta_b = 0$, until the mode's ballooning angle is shifted sufficiently (around $\theta_0 = \pi/2$) to quench the mode, after which only noise is visible. Differences between kinetic and adiabatic modes are minor. At $\hat{s} = 0.1$ (Fig. 5(b)), we again observe wider distributions in ballooning space. There is a clear distinction in these distributions between kinetic and adiabatic electron simulations. Shifting the ballooning angle merely distorts this distribution rather than quenching the mode. This is in line with the observations of the sheared case, where modes at $\hat{s} = 0.1$ could be shifted to high ballooning angles without being completely quenched, since large shifts in ballooning space correspond to comparatively low shifts in k_x.

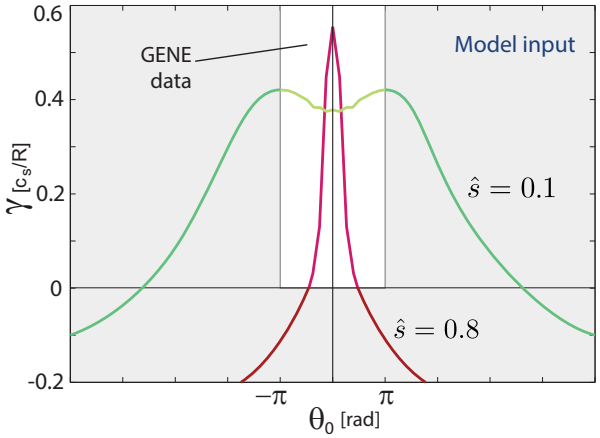

Fig. 7: Growth rate vs. ballooning angle for $\hat{s} = 0.8$ and $\hat{s} = 0.1$. The gray area is inaccessible by GENE simulations. Rotationless radial growth rates are conjectured in that region.

There is another difference between the sheared and unseared case. GENE's initial value solver only finds the most unstable mode at some radial length scale. In the unsheared ϕ_n case this most unstable mode always has $\theta_0 \in [-\pi, \pi]$. Higher k_x modes are coupled to these most unstable modes by the parallel boundary condition. Thus, by utilizing the ϕ_n method, modes left to grow at high ballooning angles always couple back to a more unstable connection with low θ_0, and as such are overwhelmed. Their structure and growth rate then can not be determined. On the other hand, these high θ_0 modes are accessible when a mode is continually sheared. The parallel boundary condition still couples these high θ_0 modes to those with low θ_0, but those connections may be quenched by the effects of flow shear. Thus, if flow shear shifts modes to high θ_0 faster than the quenched modes at low θ_0 can grow, the initial value solver indeed yields these high θ_0 modes.

The restriction on modes with the ϕ_n method is clear in Fig. 7. This figure shows the growth rate γ_n of a mode ϕ_n vs. its ballooning angle. With the initial value solver (eigenvalue calculations are problematic in the presence of flow shear), we can only access growth rates of modes with $\theta_0 \in [-\pi, \pi]$ (white area). The rest of the distribution (gray area) is guessed, based on two observations. First, it is known that in general modes become stable at higher ballooning angles, even reaching negative growth rates (reproducing the precise damping rate of the system at large ballooning angles is outside of the scope of this work). Then, the data in the white region suggests a wider distribution at low $\hat{s}$ than at high $\hat{s}$. Simple distributions obeying these two observations are utilized in the following toy model.

5 Toy Model

Many of the shown effects of flow shear on ITG modes are generally known, but not much is understood of their causes. To identify the key relations causing these effects, we now attempt capture as much of the effects as possible in a toy model. We particularly focus on reproducing mode quench, Floquet fluctuations and kinetic/adiabatic differences at high and low $\hat{s}$.

We intialize our toy model with the structures of modes ϕ_n throughout ballooning space. But as mentioned, modes at high θ_0 cannot be found with the ϕ_n method, so an assumption must be made on their shape. In this work we assume a connection between mode shape and ballooning angle, so that all ϕ_n structures periodically have the same shape as those at low θ_0, i.e. $|\phi_n(\theta_b) = \phi_{n+p}(\theta_b + 2\pi)|$, where $\phi_n = |\phi_n| e^{\gamma_n t}$ and $|...|$ indicates structures normalized to 1 (in this work $p = 16$ because of the step size choice of $\theta_0 = -\pi n/8$).

The structures ϕ_n throughout ballooning space thus have periodically the same shape but different growth rates γ_n; as shown in Fig. 7. A shifted Gaussian distribution is chosen which is narrow at high $\hat{s}$ and wide at low $\hat{s}$ and drops to negative values at large θ_0, i.e.:

$$\gamma_n = c_0 e^{-c_1 n^2} - c_2, \tag{2}$$

where an overview of constants c_j as used in the model is given in Table 1. There is litte sensitivity in the model to the precise choice of distribution function (e.g. shifted Bessel functions have been tried with similar results).

The model assumes that a dynamically sheared ITG solution Φ can be decomposed into the shearless modes ϕ_n, so that $\Phi(\theta_b, t) = \sum_{-n=\infty}^{\infty} \phi_n(\theta_b, t)$. At this point we have a model decomposition without flow shear; it only exhibits exponential growth. This is illustrated in Fig. 8.

Next these shearless modes must be coupled by some implementation of flow shear. In GENE, flow shear is implemented by shifting $\Phi(\theta_b, t)$ over the k_x grid continuously in time. In our model, at each time step, the components ϕ_n are evolved according to:

$$\begin{aligned} &\phi_n(t + \Delta t) = e^{\gamma_n \Delta t} \times \\ &\Big(\phi_n(t) - O_n(t)\phi_n(t) + O_{n+1}(t)\phi_{n+1}(t)\Big), \end{aligned} \tag{3}$$

where O_n signifies the the overlap between neighboring modes (i.e., of subsequent n):

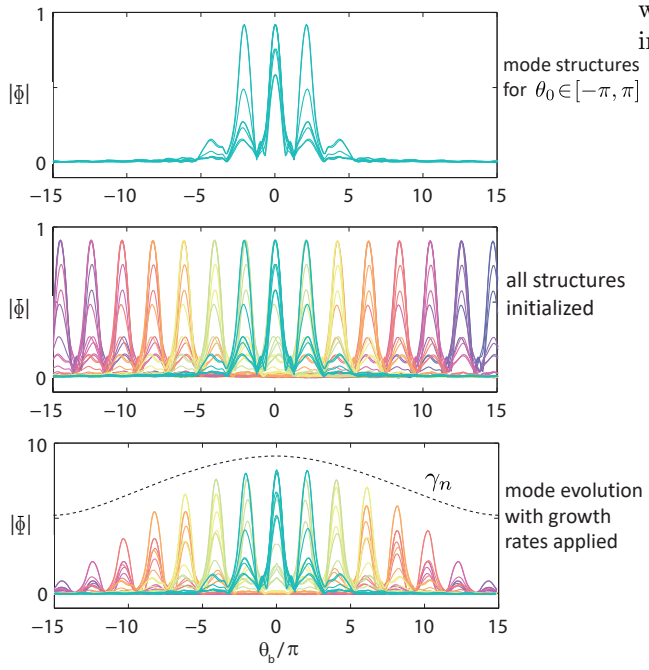

Fig. 8: Initialization and evolution of fixed-angle modes. There are 16 modes in the range $\theta_0 \in [\pi, \pi]$. These packs (given different colors) are initialized at every multiple of 2π. The modes then grow according to the chosen radial distribution function of γ_n.

$$O_n(t) = c_6 \frac{\int \mathrm{d}\theta_b \, \min[\phi_n(\theta_b), \phi_{n-1}(\theta_b)]}{\int \mathrm{d}\theta_b \, \max[\phi_n(\theta_b), \phi_{n-1}(\theta_b)]} + c_5. \tag{4}$$

Thus at each time step a mode ϕ_n obtains two terms: it yields a portion of its structure to its right neighbor and receives a fraction from its left neighbor (the asymmetry here stems from the positively chosen flow shear direction; of course this can be inverted). In essence, modes are thus slowly transformed into their neighbors at negative k_x and a general shift of the total structure towards negative ballooning space results. To speed up the calculations, these shifts do not occur at each time step, but only at each interval of $\tau_s = c_3/\gamma_E - c_4 > 0$, so that the shift rate increases with higher flow shear. This mechanism is illustrated in Fig. 9.

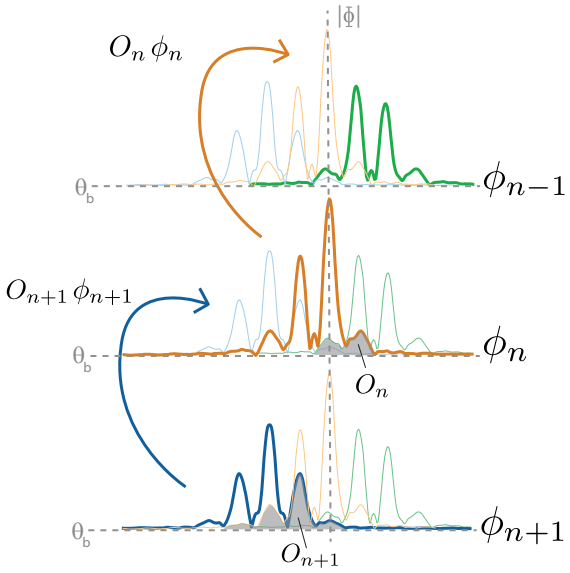

Fig. 9: Implementation of flow shear in the model: mode ϕ_n receives part of its left neighbor and gives a part of itself to its right neigbor.

One key feature of this model is that the fraction of a given mode shifted to its neighbor depends on their mutual overlap in ballooning space. When this overlap is large, the transformation by flow shear becomes more efficient. In real space, this overlap corresponds to modes which balloon at different angles, while having similar amounts of energy stored at the same radial wavelengths. Flow shear then causes energy of all wavenumbers k_x to be shifted to new ballooning angles. This process is more efficient when there is already a similar amount of energy present at those wavenumbers at the target ballooning angle. A physical motivation for this mechanism will be explored iin future work.

In Fig. 10 results of this toy model are compared to linear GENE simulations. Perturbed plasma density and corresponding growth rates are shown for several values of flow shear, at both high and low $\hat{s}$. At $\hat{s} = 0.8$, the toy model qualitatively produces all the

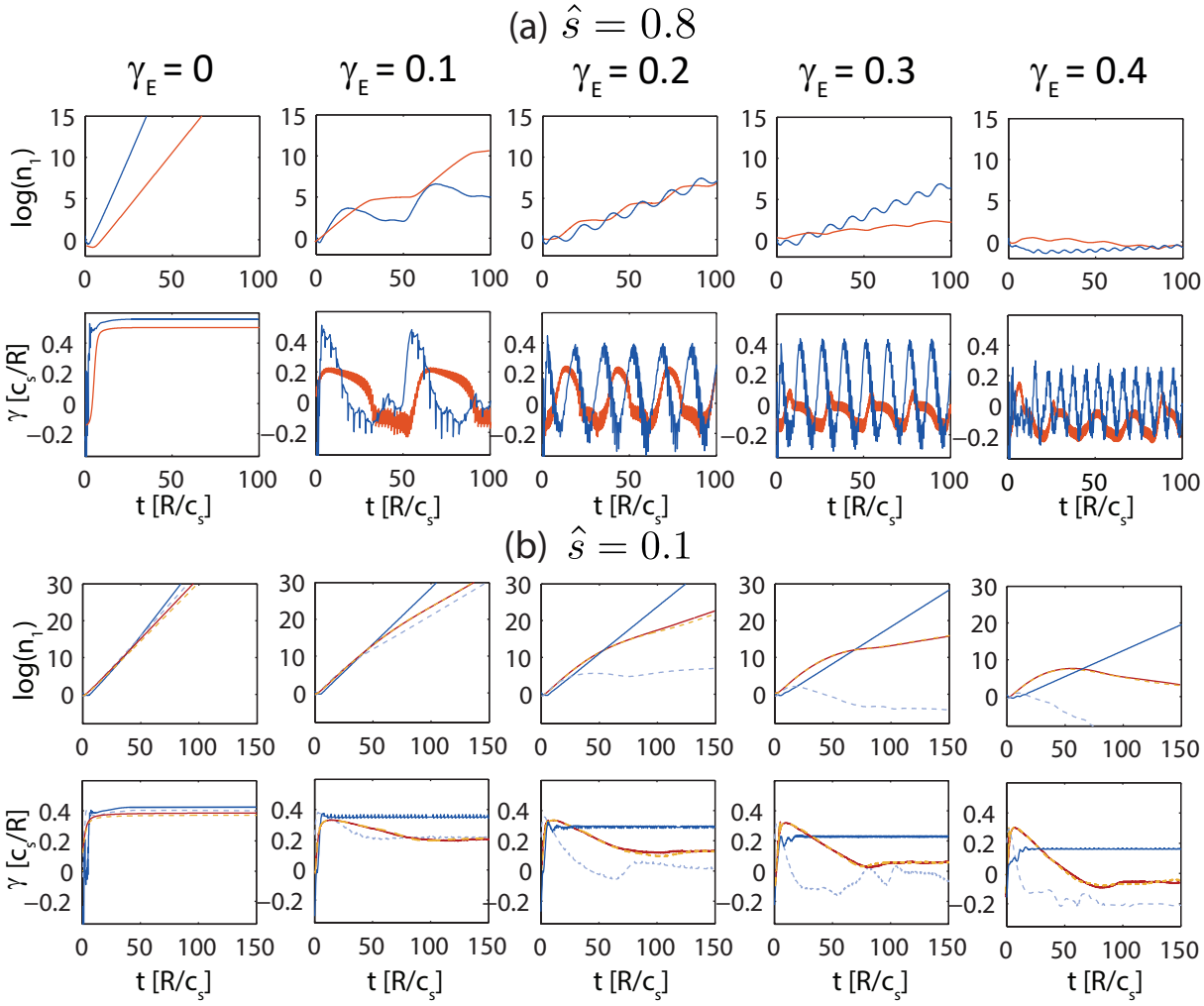

Fig. 10: Time evolution of $\log(n_1)$ and corresponding growth rates at several values of flow shear, for **(a)** $\hat{s} = 0.8$ and **(b)** $\hat{s} = 0.1$. Blue lines are GENE simulations and red lines results of the presented toy model. Solid lines correspond to kinetic electrons and dashed lines adiabatic electrons.

features that were aimed for: flow shear causes large Floquet fluctuations, and as it is increased the Floquet frequency rises and growth rates gradually drop, until at some point the mode is stabilized. Quantitatively, Floquet amplitudes and frequencies do not match; they are very sensitive to the precise combination of model parameters used. There is no kinetic/adiabatic difference. At $\hat{s} = 0.1$, general behavior is also reproduced well. The model yields no Floquet fluctuations and again a mode Φ is gradually quenched by flow shear. However, the difference between kinetic and adiabatic electron simulation that was so prevalent in GENE simulations is not captured. A more advanced model may be able to achieve this; possibly be expanding the coupling between modes (e.g., periodic coupling by the parallel boundary con-

dition instead of just nearest neighbors). This was quickly looked at but without results; more effort is needed to explore this option. With more advanced coupling it might be that the differences found in rotationless modes ϕ_n between kinetic and adiabatic mode structures could have a larger effect on the final modes Φ.

With this toy model, Floquet fluctuations can be explained by the following. All modes ϕ_n grow and receive a portion of their structure from their left neighbor ϕ_{n-1}. At some locations, overlap between two modes is very small and shifts between them thus negligible; we call this a bottleneck location. Consider such a location between ϕ_n and ϕ_{n+1} with $\gamma_{n+1} < \gamma_n$. This difference in growth may be large at $\hat{s} = 0.8$ because the γ_n radial distribution is very peaked. As such, on the left side of the bottleneck, ϕ_{n+1} will slowly start to grow by accumulated shifts which are not transfered to ϕ_n, while on the right side, ϕ_n grows quickly but also loses much of its structure (in total, there is little growth and we are at the bottom of a Floquet cycle). At some point, ϕ_{n+1} is so large that the small fraction it gives to ϕ_n is nonetheless substantial. From this point onward overlap between the modes increases and the bottleneck is removed in a snowball effect that highly boosts ϕ_n, which has a large growth rate by itself (this moment corresponds to a peak in the Floquet cycle). However, ϕ_{n+1} is now completely depleted, recreating the original bottleneck. One Floquet cycle has been completed. At low $\hat{s}$, growth rates between neighbors are rather similar, and mode structures are wider by nature. By these two properties, bottlenecks are not as pronounced and no Floquet fluctuations occur. For physical interpretation, the analogies of mode overlap and shifts were given in the previous paragraph. Next, there is the quenching impact of flow shear. This can be understood by considering the most unstable modes ϕ_n (which live around $\theta_0 = 0$). These will outgrow all other modes, and as such (on average) always yield more to their right neighbor than what they receive from the left. Modes are thus depleted proportionally to their growth rate. As flow shear is increased, shifts occur more frequently and this effect is enhanced.

Tab. 1: Declaration of constants as used in the model described in Sec. 5. The values are chosen once and kept constant throughout the simulations of this work.

Constant	Values	Relevance
n	[-240,240] (so $\theta_0 \in [-15\pi, 15\pi]$)	simulation box and mode spacing
Δt	1/8	time step
c_0	1 ($\hat{s} = 0.1$) 1.3 ($\hat{s} = 0.8$)	base growth rate
c_1	0.001 ($\hat{s} = 0.1$) 0.3 ($\hat{s} = 0.8$)	radial width of γ_n
c_2	0.3	γ_n lower bound
c_3	0.4 ($\hat{s} = 0.1$) 0.6 ($\hat{s} = 0.8$)	rate of mode shifts by γ_E
c_4	0.3 ($\hat{s} = 0.1$) 0.7 ($\hat{s} = 0.8$)	offset of γ_E-time relation
c_5	0.015	offset of O_n
c_6	0.75	mode shift amplitude

6 Summary

In this work, the ITG instability was investigated at both high and low background magnetic shear $\hat{s}$. The impact of flow shear is clearly visible there, with notable features being structures equilibrating to some shape in ballooning space (while growing/shrinking in time) and a clear difference in mode stabilization by flow shear between kinetic and adiabatic electron simulations. Next, a toy model was created, decomposing a given sheared mode Φ into shearless modes ϕ_n. The effects of flow shear are introduced by adding shifts between neighboring modes, with shift magnitude depending on the mode overlap in ballooning space. Floquet fluctuations and mode stabilization are reproduced at the appropiate scales and param-

eter ranges; indeed, it is the first time that Floquet fluctuations have been reproduced using a k_x-shift approach. However, kinetic/adiabatic electron differences are not captured.

Modeling the reduction of turbulent fluxes as a consequence of quenched linear growth rates has been validated by nonlinear simulations [10]. Furthermore, the presented toy model may provide the basis for improved quasilinear models. The QuaLiKiz [24][25] model calculates a shifted Gaussian mode structure in the presence of flow shear, which then leads to a reduction in code speed due to a loss of integration symmetry in the dispersion relation. It will be explored whether the model presented here can provide a speedup compared to the current QuaLiKiz implementation. Note that the shifted Gaussian in QuaLiKiz is necessary for momentum transport, which is not captured by this model.

However, the model is not yet ripe for such quantitative applications. It should first be expanded to yield more precise growth rates and Floquet frequencies, and then generalized to a wider parameter space (e.g., under varying q, ϵ_t, $R/L_{T\mathrm{i}}$). Finally, the model would be more powerful if it captured the difference between kinetic and adiabatic electron modes at low $\hat{s}$.

References

[1] E. J. Doyle et al., Nucl. Fusion **47**, S18 (2007)

[2] F. Romanelli, Phys. Fluids B **1**, 1018 (1989)

[3] S. C. Guo and F. Romanelli, Phys. Fluids B **5**, 520 (1993)

[4] Bourdelle C et al., Plasma Phys. Control. Fusion **58**, 014036 (2016)

[5] T. Dannert and F. Jenko, Phys. Plasmas **12**, 072309 (2005)

[6] K. H. Burrell, Phys. Plasmas **4**, 1499 (1997)

[7] P. A. Politzer et al., Nucl. Fusion **48**, 075001 (2008)

[8] H. Biglari and P. H. Diamond, Phys. Plasmas **2**, 1 (1990)

[9] S. L. Newton, S.C. Cowley, and N.F. Loureiro, Plasma Phys. Control. Fusion **52**, 125001 (2010)

[10] J.E. Kinsey, R.E. Waltz, and J. Candy, Phys. Plasmas **12**, 062302 (2005)

[11] M. Barnes et al., Phys. Rev. Let. **106**, 175004 (2011)

[12] E. G. Highcock et al., Phys. Rev. Let. **109**, 265001 (2012)

[13] J.W. Connor, R.J.Hastie, and J.B. Taylor, Phys. Rev. Let. **40**, 396 (1978)

[14] J. Candy, R.E. Waltz, and M.N.Rosenbluth, Phys. Plasmas **11**, 2514 (2004)

[15] F. Jenko, W. Dorland, M. Kotschenreuter and B.N. Rogers, Phys. Plasmas **7**, 1904 (2000); for code details and access, see http://genecode.org

[16] G. W. Hammett, W. Dorland, N.F. Loureiro, and T. Tatsuno. *Proceedings of the 48th Annual Meeting of the APS Division of Plasma Physics*, (American Physical Society, Philadelphia, 2006).

[17] R.E. Waltz et al., Phys. Plasmas **4**, 2482 (1997)

[18] E. G. Highcock et al., Phys. Rev. Let. **105**, 215003 (2010)

[19] A. J. Brizard, Rev. Mod. Phys. **79**, 421 (2007)

[20] D. Told, *Gyrokinetic Microturbulence in Transport Barriers*, Ph.D. thesis, University of Ulm (2012)

[21] C. M. Roach et al., Plasma Phys. Control. Fusion **51**, 124020 (2009)

[22] P. Cottier et al., Plasma Phys. Control. Fusion **56**, 015011 (2014)

[23] J. Citrin et al., Phys. of Plasmas **19**, 062305 (2012)

[24] C. Bourdelle et al., Phys. of Plasmas **14**, 112501 (2007)

[25] J. Citrin et al., Plasma Phys. Control. Fusion **59**, 124005 (2017)